KINETIC PROCESSES IN NEGATIVE GLOW PLASMA OF LOW PRESSURE DISCHARGE IN OXYGEN

V.V. Tsiolko, S.V. Matsevich, V.Yu. Bazhenov, V.M. Piun, A.V. Ryabtsev
Institute of Physics NAS of Ukraine, Kiev, Ukraine
E-mail: matsevich@iop.kiev.ua

It is shown that electron energy distribution function of negative glow plasma of low pressure discharge in oxygen exhibits two-temperature behavior due to the influence of metastable molecules $O_2(a^1\Delta_g)$, $O_2(b^1\Sigma^+_g)$ and excitation of O_2 vibrational levels. As well, spatial dependencies of the atomic oxygen concentration on the gas pressure and power density in the discharge plasma are determined by actinometry method.

PACS: 52.80.-s, 52.25.Ya

INTRODUCTION

At present, oxygen plasma is widely used in various technologies, such as plasma cleaning and modification of surface features of polymer materials, plasma sterilization of medical instruments, synthesis of nanostructured materials, etc [1 - 3]. In spite of complex composition of such plasma (electrons, positively charged oxygen molecule ions, neutral atoms, oxygen molecules in metastable states), exactly atomic oxygen plays dominant role in many practical applications. For measurements of atomic oxygen concentration several methods are used, including mass spectrometry, chemical titration using NO, optical absorption techniques such as LIF and TALIF, catalytic probes and such method of emission spectroscopy as actinometry [4 - 6]. Essence of this method is in adding of small known amount of actinometer gas (noble gases are commonly used) to the gas under study, and by means of measurement of intensity ratio for certain spectrum lines of actinometer gas and the component of interest, ratio of their concentrations is determined. This method is simple in implementation, it does not require costly equipment, and in principle allows real time measurements. It should be noted, however, that this method requires precise knowledge of plasma electron energy distribution function (EEDF) since the rates of excitation processes are very sensitive to EEDF shape.

In the present paper results of experimental investigations of parameters of negative glow plasma in the hollow cathode discharge in oxygen are presented. Peculiarity of such discharge consists in fact that practically whole applied voltage falls in narrow near-cathode layer, and electric field in the plasma does not exceed several Td. Gas ionization and electron heating in this case are performed by fast electron beam e_f with energy $W_f \sim 400…700$ eV, coming from the near-cathode region. Spatial distributions of EEDF shape are determined for different oxygen pressure values, and with the use of experimentally measured EEDF dependencies of atomic oxygen concentration on the system parameters are determined. As well, numerical calculations of EEDF are accomplished for the parameters corresponding to experimental conditions.

1. EXPERIMENTAL SETUP AND METHODS

Experimental setup is schematically represented in Fig. 1.

The measurements were performed in the discharge chamber having 38 cm diameter and 42 cm length, which simultaneously served as the discharge cathode, at that the discharge anode having 30.5 cm diameter was located near back side of the chamber.

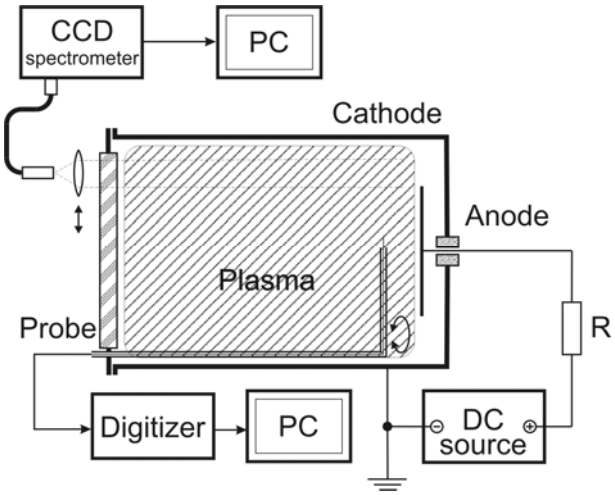

Fig. 1. Scheme of the experimental setup

The front of the chamber was closed by glass window with diameter of 26 cm. Chamber evacuation was performed by diffusion pump down to pressure of about $5 \cdot 10^{-3}$ Pa, and after that working gas was supplied to the chamber until reaching of predetermined pressure value. For excluding oil vapor coming to the discharge chamber, liquid nitrogen cooled trap was used. As working gas, either pure oxygen, or mixture of oxygen with argon (O_2 98% + Ar 2%) in case of actinometry studies was used. Working gas pressure in the chamber was varied in range of 1…16 Pa. The discharge power supply was provided by DC source with controlled voltage and current values in ranges of 400…800 V and 100…600 mA, respectively. Power introduced in the discharge varied in range of 50…350 W which corresponded to specific power in the discharge $\approx 1…7$ W/cm^3.

The plasma density, electron temperature, electron energy distribution function (EEDF) and electric field in the plasma were measured using single and double Langmuir probes made of a 100 μm tungsten wire, the length of the collecting region being 10…12 mm. The probes could be moved along and across the chamber. To avoid the effect of contamination of the probe surface on the probe current-voltage characteristic, the probes were heated to ≈ 800°C after each measurement. The probe characteristic was measured using an original PC-controlled system. The program assigned the probe current with step of 0.1 μA, and the probe voltage (with

respect to anode), the discharge voltage, and the discharge current were measured at each step. The change in the probe current at each step was calculated in real time using a special algorithm intended for optimizing the signal-to-noise ratio over the entire range of the probe currents (the total number of steps in measuring one current-voltage characteristic was 1500…2000). After measuring the probe current in a given range at a fixed discharge current and fixed discharge voltage, the data on the probe current as a function of the probe voltage with respect to the anode were stored in a PC. Measurements of the current-voltage characteristic at fixed experimental conditions were repeated 10…30 times, and the data stored in the PC were then averaged.

The EEDF was determined from the second derivative of the probe current with respect to the voltage, obtained by numerically differentiating the averaged current-voltage characteristic (by using pre-interpolation if necessary) The plasma potential was determined from the inflection point of the probe current-voltage characteristic, and the plasma density was calculated from the electron saturation current to the probe.

At determining atomic oxygen concentration by actinometry method, ratio of the emissions from the states X*/A* is proportional to the concentration ratio [X]/[A] (A and X stand for actinometer and the component of interest, respectively) when the following conditions are fulfilled:

- states X^* and A^* are formed mainly at the expense of electron excitation from ground states of the components X and A;
- X^* and A^* are deactivated mainly at the expense of emission;
- cross sections of electron excitation of X* and A* levels must have similar thresholds and shapes of dependencies on electron energy.

At determining atomic oxygen concentrations, emissions of oxygen atoms at 844.6 nm wavelength corresponding to $3p^3P \rightarrow 3s^3S^0$ transition, at 777.4 nm ($3p^5P \rightarrow 3s^5S^0$ transition) and argon atoms at 750.4 nm corresponding to $2p_1 \rightarrow 1s_2$ transition (Paschen notation) were measured. Main contribution to formation rates of oxygen excited states under consideration is provided by mechanisms of direct oxygen atom excitation by electron hit, and dissociative excitation of O_2 molecule under electron hit. It should be noted that cross section of direct excitation for O (844.6) is higher than that for O (777.4) [7]. On the contrary, contribution of dissociative excitation is higher for O (777.4) [8]. Thus, in case of O (777.4) emission, contribution of dissociative excitation is essential and can influence the obtained result. Taking into account processes of quenching of excited levels due to collisions, expressions for the emission intensities are, as follows:

$$I_{844} = C_{844}\, h\nu_{844}\, A_{ij}^{3P} n_e \frac{k_e^{3P}[O] + k_{de}^{3P}[O_2]}{\sum_j A_{ij}^{3P} + k_Q^{3P}[O_2]}, \quad (1)$$

$$I_{750} = C_{750}\, h\nu_{750}\, A_{ij}^{2p_1} n_e \frac{k_e^{2p_1}[Ar]}{\sum_j A_{ij}^{2p_1} + k_Q^{2p_1}[O_2]}, \quad (2)$$

where C is constant describing peculiarities of the optical system; ν is emission frequency; A_{ij} is Einstein coefficient for respective transition; ΣA_{ij} is a sum of Einstein coefficients for all transitions from given level; n_e is electron concentration; k_e, k_{de}, k_Q are rate constants for processes of excitation by direct electron hit, dissociative excitation, and quenching, respectively.

Rate constants are calculated using formula:

$$k = 10^2 \sqrt{\frac{2e}{m_e}} \int_{\varepsilon_0}^{\infty} \varepsilon f(\varepsilon)\sigma(\varepsilon) d\varepsilon, \quad (3)$$

where e and m_e are electron charge and mass, respectively, $\sigma(\varepsilon)$ is cross section of respective process, ε_0 is threshold energy of the process, $f(\varepsilon)$ is EEDF normalized by unity. Division of (1) over (2) gives:

$$\frac{I_{844}}{I_{750}} = C_{2p_1}^{3P} \frac{k_e^{3P}}{k_e^{2p_1}} \frac{[O]}{[O_2]} + C_{2p_1}^{3P} \frac{k_{de}^{3P}}{k_e^{2p_1}},$$

where

$$C_{2p_1}^{3P} = \frac{h\nu_{844}}{h\nu_{750}} \frac{A_{ij}^{3P}}{A_{ij}^{2p_1}} \frac{\sum A_{ij}^{2p_1} + k_Q^{2p_1}[O_2]}{\sum A_{ij}^{3P} + k_Q^{3P}[O_2]} \frac{[O_2]}{[Ar]}.$$

Following from this expression, relative atomic oxygen concentration is:

$$\frac{[O]}{[O_2]} = C_{3P} \frac{I_{844}}{I_{750}} - \frac{k_{de}^{3P}}{k_e^{3P}}, \quad (4)$$

where $C_{3P} = \frac{h\nu_{750}}{h\nu_{844}} \frac{A_{ij}^{2p_1}}{A_{ij}^{3P}} \frac{\sum A_{ij}^{3P} + k_Q^{3P}[O_2]}{\sum A_{ij}^{2p_1} + k_Q^{2p_1}[O_2]} \frac{k_e^{2p_1}}{k_e^{3P}} \frac{[Ar]}{[O_2]}$.

Similar expression can be also obtained for O(777.4) emission.

Spectrum measurements were performed by means of CCD-spectrometer SL40-2-1024USB (SOLAR TII, Minsk, Republic of Belarus). Optical system allowed collecting of the plasma emission from cylindrical region (diameter of about 1 cm) with axis aligned in parallel with the chamber one.

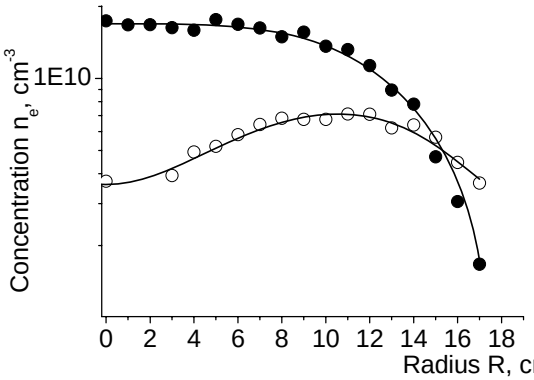

Fig. 2. Dependencies of plasma concentration n_e on the system radius R for different oxygen pressure values. Close points – P = 4 Pa, U_d = 650 V; open points P = 11 Pa, U_d = 470 V. W_d = 5 mW/cm^3

2. EXPERIMENTAL RESULTS

Fig. 2 exhibits dependencies of plasma density n_e on the system radius R for two oxygen pressure values. (The measurements were performed in the middle plane of the chamber.) One can see from the figure that radial distributions of the plasma density for those oxygen

pressure values are essentially different – at P = 4 Pa the plasma density is practically independent on R in central region of the discharge (R ≈ 0…13 cm), whereas at higher pressure the minimum of n_e value is observed at the discharge center. That is, in this case primary electrons accelerated in the cathode layer up to energy ≈ eU_d lose major portion of their energy already at medium radius value, and plasma in paraxial region is formed mainly at the expense of diffusion of particles from periphery regions.

Electron energy distribution function for different values of system radius and oxygen pressure are presented in Fig. 3,a,b. On can see from the figure that for both pressure values the EEDF possesses bi-maxwellian behavior at energy variations in range ε ≈ 0…10 eV, at that temperature of "cold" (e_c) electrons T_e1 (in energy range ε ≈ 0…2 eV) is essentially less than that of "hot" (e_h) electrons T_e2 (ε ≈ 2…10 eV).

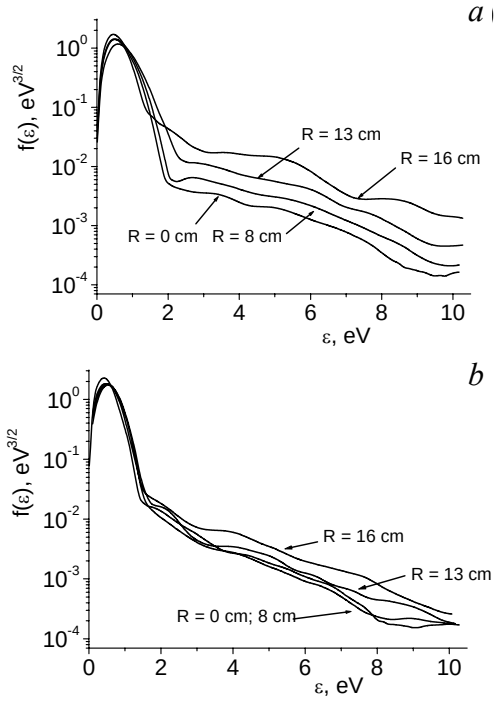

Fig. 3. Electron energy distribution function f(ε) at different system radius R for two oxygen pressure values. P = 4 Pa, U_d = 650 V (a); P = 11 Pa, U_d = 470 V (b). W_d = 5 mW/cm^3

Such EEDF shape is due to efficient excitation of metastable states $a^1\Delta_g$ and $b^1\Sigma_g^+$ of oxygen molecule having thresholds of 0.98 and 1.64 eV, respectively. It should be also noted that at 4 Pa pressure relative quantity of "hot" plasma electrons e_h (that is, those responsible for inelastic processes) has maximum at the discharge periphery, and decreases practically monotonously toward the system axis. At the same time, at 11 Pa pressure relative quantity of electrons e_h with radius R decrease from 16 to 13 cm diminishes at first, and with subsequent R decrease remains practically unchanged. Such difference in radial dependencies of EEDF shape is due to the following. At 4 Pa pressure, free run path of fast electrons e_f with respect to energy loss due to inelastic processes is essentially longer than analogous value at 11 Pa pressure (both due to decrease of concentration of oxygen molecules, and at the expense of higher electron energy W_f, proportional to U_d). In other words, fast electrons e_f at 11 Pa pressure lose the energy at their motion from the cathode toward the system center essentially faster than in case of 4 Pa pressure. Since [9] mean energy of secondary electrons ε_{sec} formed at ionization of oxygen molecules by electrons e_f diminishes with decrease of their energy W_f, it results in slower radial decrease of relative quantity of electrons e_h at 4 Pa pressure, as compared with the case of 11 Pa pressure.

One can see from radial dependencies of temperatures T_e1 and T_e2 at different oxygen pressure values (Fig. 4,a,b) that:

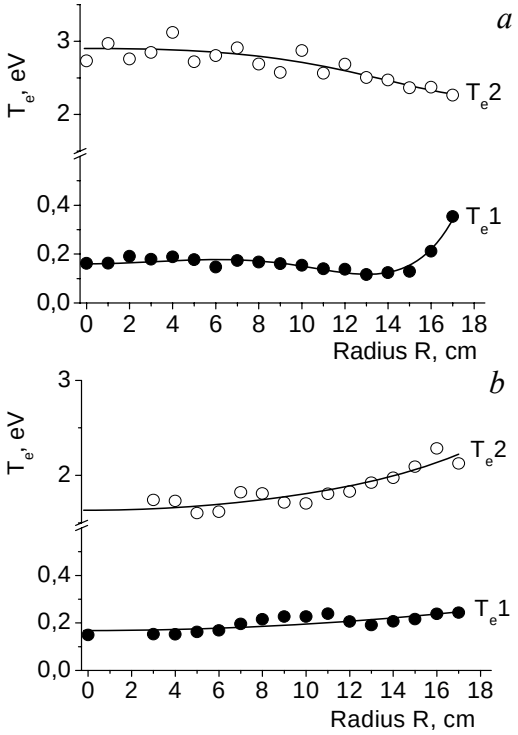

Fig. 4. Dependencies of electron temperatures T_e1 and T_e2 on system radius R for different oxygen pressure values. P = 4 Pa (a) and P = 11 Pa (b). W_d = 5 mW/cm^3

1) T_e1 in both cases comprises about 0.2 eV and is practically independent on the system radius. An exclusion is represented by R range of 15…17 cm, where at 4 Pa temperature T_e1 abruptly decreases from ≈ 0.4 eV to ≈ 0.2 eV; 2) At the same time, behavior of radial dependencies of temperature T_e2 differs with pressure variation. At P = 11 Pa T_e2 decreases toward the center from ≈ 2.3 to ≈ 1.5 eV, whereas in case of lower pressure T_e2, increase from ≈ 2.2 to ≈ 3.0 eV toward the system center is observed. Decrease of T_e2 toward the system center at 11 Pa pressure is due to quick spatial relaxation of energy of fast electrons e_f and, respectively, with decrease of mean energy of electrons ε_{sec}. Certain growth of T_e2 toward the discharge center at 4 Pa is possibly due to fact that, resulting from cylindrical geometry of the discharge cathode, density of fast electrons e_f increases toward the system axis, which in turn leads to "heating" of electrons e_h. At the same time, at 4 Pa pressure (as well as at 11 Pa) mean energy of plasma electrons, as a whole, decreases toward the discharge axis (Fig. 5)

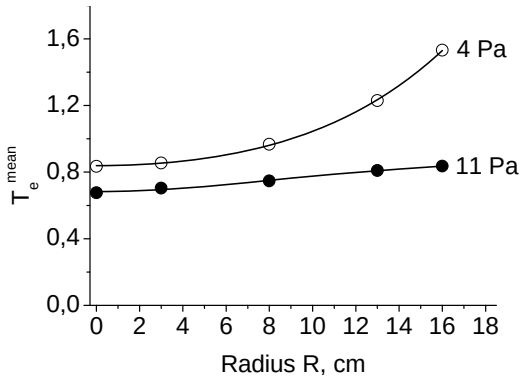

Fig. 5. Dependencies of mean energy of plasma electrons T_e^{mean} on the system radius R for different oxygen pressure values. W_d = 5 mW/cm^3

Longitudinal electric field in main region of the discharge plasma does not exceed ≈ 5 mV/cm and weakly depends on the system radius. At the same time, radial dependence of radial component of electric field E_r has non-monotonous behavior – while exhibiting growth in a whole with increase of the system radius, E_r consequently passes local maximum and minimum with their radial locations being dependent on oxygen pressure. E_r value shows certain growth with pressure decrease and at middle system radius is about 15…25 mV/cm. As a whole, at 4 Pa pressure absolute electric field value $|E|$ is in range ≈ 1.5…4.5 Td, and at 12 Pa pressure - ≈ 0.5…1.5 Td.

In calculations of atomic oxygen concentrations at different discharge parameters by means of expression (4) cross sections and rates of processes taken from [7, 8, 10, 11] were used. Determining of rates of the processes (3) was accomplished with the use of experimentally defined EEDF, approximated up to energy value of 50 eV. As well, it was supposed that gas temperature in considered ranges of variations of pressure and specific power comprised about 400…450 K.

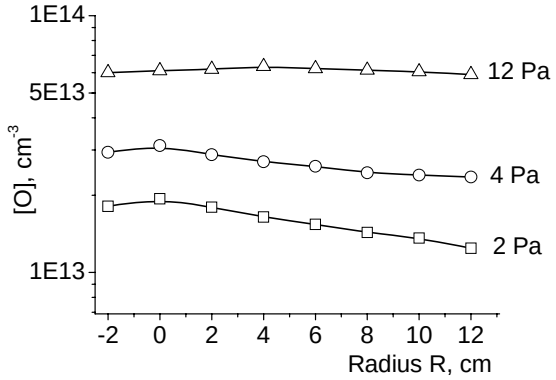

Fig. 6. Radial dependencies of atomic oxygen concentration [O] (obtained by means of I_{844}/I_{750} ratio) in the discharge plasma for different oxygen pressure values. W_d = 5 mW/cm^3

Fig. 6 exhibits radial dependencies of atomic oxygen concentration [O] at different pressure values P obtained with the use of I_{844}/I_{750} ratio. One can see from the figure that at low pressure values (2 and 4 Pa) [O] increases toward the system center, that is in a whole reproduces n_e radial dependence (although spatial rate of the increase is somewhat lower). At the same time, at 12 Pa atomic oxygen concentration is practically independent on the system radius, although plasma density in this case has distinct minimum at the axis. Since temperature T_e2 in this case also decreases toward the system axis, possible reason for such "flattening" of [O] dependence is due to diffusion of atomic oxygen toward the system center. One can also see from the figure that at pressure growth, simultaneously with [O] increase, oxygen dissociation degree $[O]/[O_2]$ decreases. Particularly, at 2 Pa pressure the degree of dissociation at the system axis is ≈ 4.5%, whereas pressure increase up to 12 Pa leads to $[O]/[O_2]$ decrease down to ≈ 2.5%.

Behavior of [O] radial dependence at the discharge specific power variation is practically unchanged. One can see from Fig. 7 that at 12 Pa [O] at the system axis remains practically the same with specific power variation, whereas [O] growth is observed at lower pressure values.

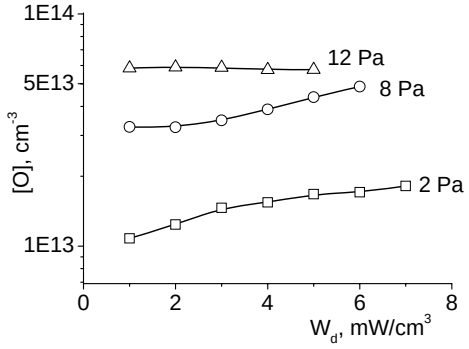

Fig. 7. Dependencies of atomic oxygen concentration [O] (obtained with the use of I_{844}/I_{750} ratio) at the system axis on specific power in the discharge W_d for different oxygen pressure values

Analogous dependencies of [O] on the system parameters were also obtained in case of use of intensity ratio I_{777}/I_{750}. However, oxygen concentration values obtained in this case were several times higher. It is possibly due to neglecting other processes of atomic oxygen formation (particularly, dissociation of metastable molecules O_2, which may provide essential influence on [O] calculation by means of I_{777}/I_{750} ratio) or incorrect approximation of EEDF behavior from energy range ε = 0…10 eV to higher energy values, since calculation of the rates of excitation processes requires exact knowledge of high energy portion of the EEDF. Unfortunately, method of Langmuir probes does not allow precise measurements of EEDF shape for energy values above 10…15 eV, and for this reason EEDF calculations were performed for comparison with experimental data.

3. CALCULATIONS AND DISCUSSION

For determining EEDF appearance, Boltzman equation is solved in two-term approximation [12]. At that, transport cross section for electron scattering on oxygen molecules is taken from [11], and main processes taken into account in the integral of inelastic collisions are listed in Table. In our model we consider that one half of power introduced into the discharge is spent on oxygen ionization in the discharge volume, and this ionization occurs homogeneously in the whole discharge volume with rate $w/(2\varepsilon_i)$, where w is specific power introduced into the discharge, and ε_i is oxygen ionization energy (12,2 eV). Energy distribution of secondary electrons is taken proportional to $1/(\varepsilon_s^2+\varepsilon_0^2)$, where ε_s is

secondary electron energy, and $\varepsilon_0 = 17.4$ eV is parameter, which is close to actual distribution [7].

N	Reactions	Threshold, eV	Ref.
1	$O_2 + e \rightarrow O_2(v) + e$	0.195	11
2	$O_2 + e \rightarrow O_2(^1\Delta_g) + e$	0.98	13
3	$O_2 + e \rightarrow O_2(b^1\Sigma_g^+) + e$	1.64	13
4	$O_2 + e \rightarrow O_2(A^3\Sigma_u^+) + e$	4.5	11
5	$O_2 + e \rightarrow O_2^* + e$	6.0	13
6	$O_2 + e \rightarrow O_2^+ + e + e$	12.2	7
7	$O_2 + e \rightarrow O + O^-$	3.6	11

One can see from Fig. 8 that, as it was expected, two-temperature EEDF behavior in energy range of ≈ 0…10 eV is, first of all, due to influence of excitation of metastable states and vibrational levels of O_2. At the same time, one can see that calculated EEDF exhibits a bend not only at energy ≈ 2 eV, but as well, at about 10 eV, at that temperature/mean energy of electrons at energy values > 10 eV is several times higher than temperature T_e2. Such EEDF behavior may be a reason for discrepancy in measured [O] values.

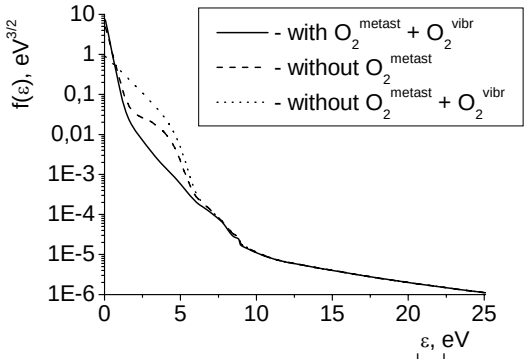

Fig. 8. Calculated EEDF. P = 12 Pa, $|E| = 1$ Td

REFERENCES

1. U. Cvelbar, M. Mozetic, and M. Klanjsek-Gunde. Selective Oxygen Plasma Etching of Coatings // *IEEE Transactions On Plasma Science*. 2005, v. 33, № 2, p. 236.
2. T. Gokus, R.R. Nair, et al. Making Graphene Luminescent by Oxygen Plasma Treatment // *ACS Nano*. 2009, v. 3, p. 3963-3968.
3. D.B. Graves. The emerging role of reactive oxygen and nitrogen species in redox biology and some implications for plasma applications to medicine and biology // *J. Phys. D: Appl. Phys.* 2012, v. 45, p. 263001.
4. J.W. Coburn, M. Chen. Optical emission spectroscopy of reactive plasmas: A method for correlating emission intensities to reactive particle density // *J. Appl. Phys.*1980, v. 51, p. 3134.
5. R.E. Walkup, K.L. Saenger, G.S. Selwyn. Studies of atomic oxygen in O_2+CF_4 RF discharge by two-photon laser-induced fluorescence and optical emission spectroscopy // *J. Chem Phys*. 1986, v. 84, p. 2668.
6. N.S. Fuller, M.V. Malyshev, V.M. Donelly, I.P. Herman. Characterization of transformer coupled oxygen plasmas by trace rare gases-optical emission spectroscopy and Langmuir probe analysis // *Plasma Sources Science and Technology*. 2000, v. 9, p. 116-127.
7. R.R. Laher, F.R. Gilmore. Updated excitation and ionization cross sections for electron impact on atomic oxygen // *J. Phys. Chem. Ref. Data*. 1990, v. 19, p. 277.
8. M.B. Schulman, F.A. Sharpton, S. Shung, C.C. Lin, L.W. Anderson. Emission from oxygen atoms produced by electron-impact dissociative excitation of oxygen molecules // *Phys. Rev. A*. 1985, v. 32, p. 2100.
9. C.B. Opal, E.C. Beaty, W.K. Peterson. Tables of secondary-electron-production cross sections // *Atomic Data.* 1972, v. 4, p. 209-253.
10. M. Hayashi. Bibliography of electron and photon cross sections with atoms and molecules published in the 20th century – Argon // *NIFS Data – 72*. 2003, p. Argon 4.
11. Y. Itikawa, A. Ichimura, K. Onda, et al. Cross-sections for collisions of electron and photons with oxygen molecules // *J. Phys. Chem. Ref. Data*. 1989, v. 18, № 1, p. 23-42
12. P.M. Golovinsky, V.P. Goretsky, A.V. Ryabtsev, et al. Influence of cesium on the emission of hydrogen negative ions from the reflective discharge source // *Zh. Tech. Fiz*. 1991, v. 61, № 10, p. 46-52 (in Russian).
13. R. Higgins, C.J. Noble, P.G. Burke. Low energy electron scattering by oxygen molecules // *J. Phys. B: At. Mol. Opt. Phys.* 1994, v. 27, p. 3203-3216.
14. H.C. Straub, P. Renault, B.G. Lindsay, et al. Absolute partial cross sections for electron-impact ionization of H_2, N_2, and O_2 from threshold to 1000 eV // *Physical Review A*. 1996, v. 54, № 3, p. 2146-2153.

Article received 05.04.2013.

КИНЕТИЧЕСКИЕ ПРОЦЕССЫ В ПЛАЗМЕ ОТРИЦАТЕЛЬНОГО СВЕЧЕНИЯ РАЗРЯДА НИЗКОГО ДАВЛЕНИЯ В КИСЛОРОДЕ

В.В. Циолко, С.В. Мацевич, В.Ю. Баженов, В.М. Пиун, А.В. Рябцев

Показано, что функция распределения электронов по энергиям плазмы отрицательного свечения разряда низкого давления в кислороде имеет двутемпературный характер из-за влияния метастабильных молекул $O_2(a^1\Delta_g)$, $O_2(b^1\Sigma^+_g)$ и возбуждения колебательных уровней O_2. Методом актинометрии установлены пространственные зависимости концентрации атомарного кислорода от давления газа и удельной мощности в разряде.

КІНЕТИЧНІ ПРОЦЕСИ В ПЛАЗМІ НЕГАТИВНОГО СВІТІННЯ РОЗРЯДУ НИЗЬКОГО ТИСКУ В КИСНІ

В.В. Ціолко, С.В. Мацевич, В.Ю. Баженов, В.М. Піун, А.В. Рябцев

Показано, що функція розподілу електронів по енергіях плазми негативного світіння розряду низького тиску в кисні має двотемпературний характер із-за впливу метастабільних молекул $O_2(a^1\Delta_g)$, $O_2(b^1\Sigma^+_g)$ та збудження коливальних рівнів O_2. Методом актинометрії встановлено просторові залежності концентрації атомарного кисню від тиску газу та питомої потужності в розряді.